Journal of Magnetism and Magnetic Materials 480 (2019) 87–96

Contents lists available at ScienceDirect

Journal of Magnetism and Magnetic Materials

journal homepage: www.elsevier.com/locate/jmmm

Research articles

Size-defined synthesis of magnetic nanorods by *Salvia hispanica* essential oil with electromagnetic excitation properties useful in microwave imagining

Anna Dzimitrowicz[a,*], George C. diCenzo[b], Przemyslaw Swatek[c], Piotr Cyganowski[d], Agata Stencel[a], Dorota Pogoda[e], Piotr Jamroz[a], Pawel Pohl[a]

[a] Wroclaw University of Science and Technology, Faculty of Chemistry, Department of Analytical Chemistry and Chemical Metallurgy, Wybrzeze St. Wyspianskiego 27, 50-370 Wroclaw, Poland
[b] University of Florence, Department of Biology, Via Madonna del Piano 6, 500-19 Sesto Fiorentino, Italy
[c] Polish Academy of Science, Institute of Low Temperature and Structural Research, Okolna 2, 50-950 Wroclaw, Poland
[d] Wroclaw University of Science and Technology, Faculty of Chemistry, Department of Polymer and Carbonaceous Materials, Wybrzeze St. Wyspianskiego 27, 50-370 Wroclaw, Poland
[e] Wroclaw University of Science and Technology, Faculty of Chemistry, Department of Inorganic and Structural Chemistry, Wybrzeze St. Wyspianskiego 27, 50-370 Wroclaw, Poland

ARTICLE INFO

Keywords:
Chia
Ferrofluids
Magnetic materials
Iron oxide
Microwave-imaging
Nanostructures

ABSTRACT

Salvia hispanica (chia) essential oil was applied for successful production of magnetic nanorods. The influence of several parameters, *i.e.* temperature of the reaction mixture, volume of the *S. hispanica* essential oil solution, stirring speed of the reaction mixture, and flow rate of the N_2 protective gas, on their axial length was studied. A design of experiments (DOE) approach followed by the response surface methodology (RSM) identified the optimal conditions for synthesis of ~3 nm magnetic nanorods. The granulometric and magnetic properties of these magnetite nanorods were analyzed using transmission electron microscopy (TEM), energy dispersive X-ray scattering (EDX), selected area electron diffraction spectroscopy (SAED), X-ray diffraction (XRD), and superconducting quantum interference device (SQUID) magnetometer. These methods revealed that the produced magnetic nanorods had a crystalline cubic inverse spinel structure with an average axial length of 43.4 ± 20.5 nm, diameter of 3.6 ± 0.9 nm, and aspect ratio of 12.1 ± 5.2 nm, and they suggested the presence of spin glass-like (mictomagnetic) behavior with both ferro- and antiferromagnetic interactions. In addition, attenuated total reflectance Fourier transform infrared spectroscopy (ATR FT-IR) was used to identify functional groups of the organic compounds present in *S. hispanica* essential oil that were possibly responsible for production and surface functionalization of the magnetite nanorods. The resultant magnetic nanofluid displayed electromagnetic excitation when exposed to microwave radiation, and therefore it could be useful in microwave-imaging of tissues.

1. Introduction

There is high scientific interest in the production and characterization of nanomaterials due to their unique optical, physicochemical, mechanical, thermal, and magnetic properties [1]. Magnetic magnetite (Fe_3O_4) nanostructures are commonly applied as adsorbents of dyes [2], carriers of drugs in drug delivery systems [3], biosensors for DNA detection [4], catalysts in chemical reactions [5], and as data storage media in electronics [6]. They have also gained interest in the medical field due to their potential use as anti-tumor agents in controlled magnetic fluid hyperthermia [7] or contrast agents in magnetic resonance imaging (MRI) [8]. In addition, Fe_3O_4 nanostructures are biocompatible and hence they can be used in clinical procedures, which makes them extraordinary appealing. Unfortunately, MRI techniques, although popular, suffer from various drawbacks, including high costs, low availability, and high rates of false results, especially in breast cancer imaging [9]. For these reasons, additional interest is given to improving diagnostic methodologies that involve Fe_3O_4 nanostructures as contrast agents. Among them, microwave excitation of magnetite nanostructures is particularly important because microwave radiation provides essential information about the morphology of various tissues [10,11].

* Corresponding author.
E-mail addresses: anna.dzimitrowicz@pwr.edu.pl (A. Dzimitrowicz), georgecolin.dicenzo@unifi.it (G.C. diCenzo), p.swatek@int.pan.wroc.pl (P. Swatek), piotr.cyganowski@pwr.edu.pl (P. Cyganowski), dorota.pogoda@pwr.edu.pl (D. Pogoda), piotr.jamroz@pwr.edu.pl (P. Jamroz), pawel.pohl@pwr.edu.pl (P. Pohl).

https://doi.org/10.1016/j.jmmm.2019.02.056
Received 29 December 2018; Received in revised form 12 February 2019; Accepted 18 February 2019
Available online 19 February 2019
0304-8853/

Several alternative and green synthesis methods for production of magnetite nanostructures have been developed and described in the literature [2,8,12–23]. These methods are environmentally friendly because no toxic by-products are formed and no toxic substrates are used for synthesis. In addition, most of them are fast and allow for the production of nanostructures of tailored size and shape [2,8,12–23]. Nanostructures produced with the aid of the above-mentioned methods facilitate their surface functionalization and biocompatibility, making them a versatile tool in modern bionanotechnology. These methods rely upon different natural products, *i.e.,* plant extracts [2,14–17,19–23], seaweed extracts [8,13,18,21], and sugars [12,15], for synthesis and stabilization of magnetic nanostructures. To the best of our knowledge, only a few studies attempted to optimize the reaction process by considering the influence of different experimental conditions, particularly the reducing agent concentration [15,17], temperature [21], and pH [21] of the reaction mixtures, on the size and magnetic properties of the resultant nanostructures. Furthermore, most of methods cited above focused on production of spherical [12–14,16,19–21,23], rectangular [15], cubic [8], and irregular-shaped [17] magnetite nanostructures. Little attention has been paid to the fabrication of rod-shaped Fe_3O_4 nanostructures [2,22]. The main advantage of magnetite nanorods, as compared to magnetite nanostructures of other shapes, is their higher specific absorption rate of radiation and better heating [24]. These features make them exceptionally appealing in microwave-assisted imaging because it could be expected that they might reveal improved magnetic excitation for advanced breast cancer imaging [25].

Salvia hispanica, better known as chia, is normally grown for human and animal feeding in several regions of the Americas. Chia seed oil is also commonly used as a nutritional supplement and a beauty product largely due to the high concentrations of omega-3 fatty acids [26] as well as terpenes and sesquiterpenes, *i.e.,* widdrol, globulol, γ-muurolene, β-pinene, β-caryophyllene, β-bourbonene, linalool, valencene, x-τcadinol, α-humulene, and germacrene-B [27]. The composition of *S. hispanica* essential oil, and its widespread availability, makes it an interesting candidate as a reducing and capping agent in novel and economically profitable green synthesis of biogenic magnetic nanostructures, complementing the use of other plant extracts in the green synthesis and surface functionalization of metallic nanoparticles [28–33].

The main objectives of the present study were to *i)* examine the suitability of *S. hispanica* essential oil to serve as reducing and capping agents in size-controlled synthesis of magnetic nanorods, and *ii)* evaluate the usability of the resulting magnetic nanofluids in microwave-assisted imaging of tissues. Design of Experiments (DOE) followed by response surface methodology (RSM) were applied for multivariate optimization of the experimental conditions of green synthesis of magnetite nanorods and selection of proper conditions under which size-defined nanorods were produced. The response of the system was the size of magnetic nanorods as determined in reference to their axial length using dynamic light scattering (DLS). On the basis of the full quadratic regression model, the experimental conditions producing magnetic nanorods with an axial length of ~3 nm were chosen. The morphology and crystal structure of the magnetic nanorods were assessed using transmission electron microscopy (TEM), energy dispersive X-ray spectroscopy (EDX), selected area electron diffraction (SAED), and X-ray diffraction (XRD). The magnetic properties of the resultant magnetic nanorods were evaluated using a superconducting quantum interference device (SQUID) magnetometer. Additionally, interactions between *S. hispanica* essential oil and the surface of the synthesized nanostructures were examined by attenuated total reflectance Fourier transform infrared spectroscopy (ATR FT-IR). Finally, the thermal behavior of the obtained magnetite nanofluids in a microwave radiation field was examined to reveal their response to dielectric heat.

2. Materials and methods

2.1. Reagents and solutions

All reagents were of analytical grade or better. Re-distilled water was used throughout. Iron(III) chloride hexahydrate ($FeCl_3{\cdot}6H_2O$) and iron(II) chloride tetrahydrate ($FeCl_2{\cdot}4H_2O$) were purchased from Sigma-Aldrich (Steinheim, Germany). *S. hispanica* essential oil was obtained from a local company. Pure (99.996%) N_2 protective gas was supplied by Messer (Wroclaw, Poland). Reaction mixtures were prepared as follows. One gram of $FeCl_3{\cdot}6H_2O$ and half a gram of $FeCl_2{\cdot}4H_2O$ were dissolved in three mL of re-distilled water, resulting in a Fe(III) and Fe(II) ions ratio of approximately 1.5. The 3.0 mL resulting solution was then mixed with an appropriate volume (3.0 mL, 4.0 mL, 5.0 mL) of *S. hispanica* essential oil, and re-distilled water was added up to 8.0 mL.

2.2. Multiparameter optimization of magnetic nanostructures synthesis

To optimize the synthesis process of biogenic magnetic nanostructures and to select appropriate parameters so as to achieve nanorods of predefined sizes, DOE with RSM were applied. Accordingly, the Box-Behnken response surface design was used to plan experimental treatments for the system, considering the following four parameters at three different levels (−1, 0, +1): reaction mixture temperature (A: 20 °C, 60 °C, 100 °C), *S. hispanica* essential oil concentration in the reaction mixture (B: 37.5%, 50.0%, 62.5% [v/v]), stirring speed of the reaction mixture (C: 0 rpm, 500 rpm, 1000 rpm), and the N_2 (protective gas) flow rate percolated through the reaction mixture (D: 0 mL min^{-1}, 150 mL min^{-1}, 300 mL min^{-1}). Ranges of experimental parameters were selected based on preliminary tests aimed at identifying the conditions under which magnetic nanostructures were produced. The planned response surface design included 27 randomized experimental treatments, including three center points. The response of the system, *i.e.,* average size of the fabricated magnetite nanorods in reference to their axial length, was measured by DLS and evaluated using Minitab18 software for Windows 7 (32 bit). All experimental treatments were carried out in a single block. Actual and coded values of all experimental parameters for the above-mentioned response surface design are given in Table 1, along with established values of the response of the system.

The synthesis was performed according to the conditions set in the response surface design matrix. Following the mixing of *S. hispanica* essential oil and the Fe(III)/Fe(II) ion solution, the synthesis of the magnetic nanostructures took place at the interface of the two phases, *i.e.,* the aqueous solution and the organic essential oil. The reaction mixtures were either stirred (500 or 1000 rpm) to mix both phases, or left unstirred (Fig. 1). The time of synthesis was 10 min and was arbitrarily selected, observing formation of magnetic nanorods (Fig. 1). The synthesis was temperature-controlled by placing reaction vials into a water bath having a temperature of 20, 60, or 100 °C (Fig. 1). The essential oil phase was enriched with the produced nanostructures because its color turned black (as shown in Fig. 1), which is characteristic for magnetic Fe_3O_4 nanofluids [34]. Freshly fabricated magnetite nanostructures were separated from the reaction mixtures by magnetic decantation, then washed with water several times, and finally re-dispersed in water as reported elsewhere [35].

The DLS measurements were carried out approximately 50 h after synthesis using a Photocor Complex device (Photocor Instruments, Tallin, Estonia) supported by a 657 nm laser (power of 28 mW) and a 288-channel autocorrelator. Scattering angle of the light beam was set at 90°. All measurements of solutions containing magnetic nanorods were performed using 148-mm round cells at surrounding air temperature, *i.e.,* 299 K (± 0.05 K). The results of these measurements, including particle size distribution, were analyzed using DYNALS software (version 2.8.3). The sizes of the synthesized magnetic nanorods in

Table 1
The Box-Behnken response surface design matrix with actual and coded values of the experimental parameters for the synthesis of magnetic nanostructures, as well as the response of the system, *i.e.* the average axial length as measured by dynamic light scattering (DLS). The following parameters were considered in the matrix: reaction mixture temperature (A, in °C), essential oil volume added to the solution of magnetic nanorods precursors (B, in mL), stirring speed of the reaction mixture (C, in rpm), and N_2 flow rate passed through the reaction mixture (D, in mL min^{-1}).

Run order	Actual and (coded) levels of the experimental parameters				Response (average size, nm)
	A (in °C)	B (in mL)	C (in rpm)	D (in mL min^{-1})	
1	20 (−1)	4.0 (0)	0 (−1)	150 (0)	344.0
2	20 (−1)	4.0 (0)	500 (0)	150 (0)	12.2
3	100 (+1)	4.0 (0)	0 (−1)	150 (0)	75.0
4	60 (0)	4.0 (0)	1000 (+1)	0 (−1)	73.2
5	60 (0)	3.0 (−1)	0 (−1)	150 (0)	309.5
6	20 (−1)	4.0 (0)	500 (0)	300 (+1)	55.5
7	60 (0)	3.0 (−1)	500 (0)	0 (−1)	19.6
8	100 (+1)	4.0 (0)	500 (0)	300 (+1)	63.6
9	60 (0)	4.0 (0)	0 (−1)	0 (−1)	4.4
10[a]	60 (0)	4.0 (0)	500 (0)	150 (0)	36.9
11	100 (+1)	4.0 (0)	1000 (+1)	150 (0)	31.4
12	60 (0)	4.0 (0)	0 (−1)	300 (+1)	10.2
13	20 (−1)	4.0 (0)	500 (0)	0 (−1)	34.5
14	100 (+1)	5.0 (+1)	500 (0)	150 (0)	19.6
15	20 (−1)	4.0 (0)	1000 (+1)	150 (0)	71.0
16	60 (0)	5.0 (+1)	500 (0)	0 (−1)	35.5
17	60 (0)	5.0 (+1)	0 (−1)	150 (0)	46.9
18	60 (0)	5.0 (+1)	500 (0)	300 (+1)	42.0
19	60 (0)	4.0 (0)	1000 (+1)	300 (+1)	32.8
20[a]	60 (0)	4.0 (0)	500 (0)	150 (0)	49.2
21	20 (−1)	3.0 (−1)	500 (0)	150 (0)	3.0
22	60 (0)	3.0 (−1)	1000 (+1)	150 (0)	8.4
23[a]	60 (0)	4.0 (0)	500 (0)	150 (0)	100.0
24	60 (0)	5.0 (+1)	1000 (+1)	150 (0)	30.6
25	100 (+1)	4.0 (0)	500 (0)	0 (−1)	13.5
26	100 (+1)	3.0 (−1)	500 (0)	150 (0)	38.4
27	60 (0)	3.0 (−1)	500 (0)	300 (+1)	38.3

[a] Center points (A = 0, B = 0, C = 0, D = 0).

reference to their axial length were calculated on the basis on the CONTIN algorithm [36].

2.3. Characterization of granulometric properties of magnetic nanostructures

The size, shape, and elemental composition of magnetic nanostructures synthesized under optimal experimental conditions, as selected on the basis of DOE and RSM, were determined using TEM (Tecnai $G^2$20 X-TWIN, FEI, Hillsboro, OR, USA), supported by an EDX instrument (FEI, Hillsboro, OR, USA). To perform TEM measurements, one drop of synthesized magnetite nanofluid (50 μL) was placed onto a Cu grid mesh (CF 400 Cu-UL, Electron Microscopy Sciences, Hatfield, PA, USA) and evaporated in air. The axial lengths and diameters of the nanorods were determined based on the measurements of 80 single nanostructures using FEI software (version 3.2 SP6 build 421, FEI, Hillsboro, OR, USA). These values were used to calculate their aspect ratio (length to diameter).

To determine the crystalline structure of the nanostructures, SAED and XRD were used. The SAED measurement was carried out during TEM analyses, maintaining the above-described preparation procedure. The XRD studies were performed in the symmetric Θ/2Θ Bragg-Brentano geometry using a X-Pert Pro MPD diffractometer (Malvern Panalytical, Malvern, United Kingdom) equipped with a CuK α radiation source (λ = 0.15406 nm). An appropriate portion of the magnetic nanofluid was placed onto poly(methylmetacrylate) holder, and dried in air.

2.4. Characterization of magnetic properties of magnetic nanorods

Temperature and magnetic-field dependencies of the magnetic nanostructures synthesized in optimal experimental conditions were performed from 1.8 to 400 K in external magnetic fields up to 7 T with a commercial SQUID magnetometer, Quantum Design MPMS-7 (San Diego, CA, USA). In order to prevent physical motion of the powders, obtained after evaporation of magnetic nanofluids, in response to the magnetic field, they (30 mg) were pressed into pellets that were later on rigidly placed in a capsule, and suspended in a straw. The background coming from the weakly diamagnetic sample holder was found to be negligible as compared to the total magnetic signal measured, so its subtraction was omitted.

2.5. The role of chemical compounds in synthesis of magnetic nanorods

ATR FT-IR spectroscopy was used to identify the chemical composition of *S. hispanica* essential oil, as well as to distinguish functional groups that might be responsible for the synthesis, stabilization, and surface functionalization of the magnetic nanostructures. ATR FT-IR spectra of pure *S. hispanica* essential oil and the organic phase after synthesis that contained used *S. hispanica* essential oil and the resultant magnetic nanorods were recorded in the range from 4000 to 370 cm^{-1} with a resolution of 4 cm^{-1} and involved 64 scans. A Vertex 70v FT-IR spectrophotometer (Bruker, Bremen, Germany) equipped with a diamond ATR cell was used to acquire these ATR FT-IR spectra.

2.6. Thermal behavior of magnetic nanorods in the microwave radiation field

An ERTEC 02-02 microwave reactor (Wroclaw, Poland) was used and set to a power of 40 W for 5 min. The magnetic nanofluid (or water as control) was diluted with re-distilled water to a final volume of 20 mL. Then, it was introduced into a glass reaction chamber. Microwave power delivered to the system and temperature of the chamber was monitored on-line. Both variables were used in a

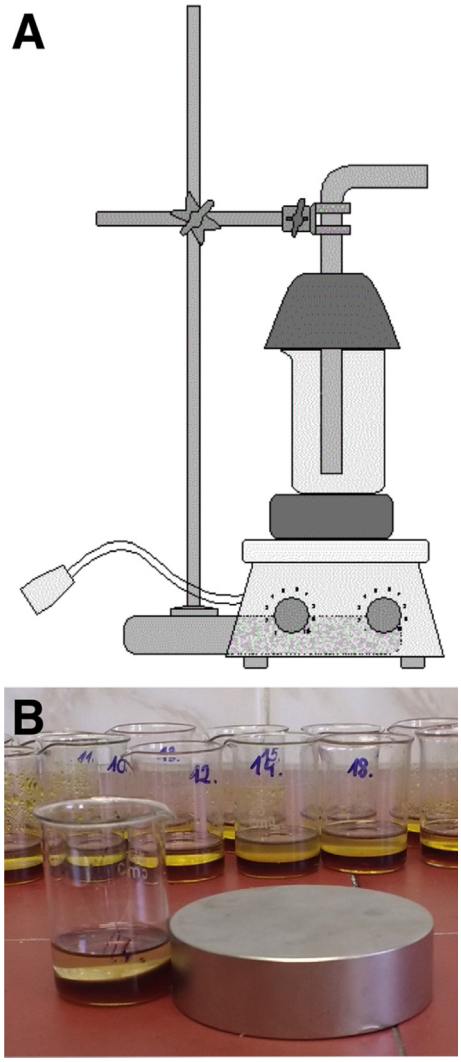

Fig. 1. (A) A schematic representation of the system used for *S. hispanica* mediated green synthesis of magnetic nanorods. (B) The colour of the solution after the synthesis process. (For interpretation of the references to color in this figure legend, the reader is referred to the web version of this article.)

simplified version of Newton's law of heating/cooling, which links the temperature of a heated liquid and the surrounding environment [37]. The thermal behavior of the system was assessed with the model defined as: $dT(t)/dt = k(h) \times \Delta T(t)$, where T(t) is temperature at given time; k(h) is the heating rate (s^{-1}), and ΔT(t) is a difference in temperature over time t.

3. Results and discussion

3.1. Evaluation of the response surface regression model

To understand the effects of the studied parameters on the size (axial length) of the magnetic nanostructures, the average size of the magnetic nanorods was modeled with a complete quadratic function, including the main and quadratic effects as well as two-way interactions. To reduce complexity of the model for easier interpretation, insignificant terms were eliminated using the *backward-elimination-of-terms* algorithm. The equation of this model is as follows (given in uncoded values):

$$\text{average size (in nm)} = 602 - 1.98\ A - 88\ B - 1.03\ C + 2.00 \times 10^{-4}\ C^2 + 2.87 \times 10^{-3}\ AC + 1.42 \times 10^{-1}\ BC$$

Table 2
Analysis of variance (ANOVA) and *lack-of-fit* test for the response surface regression model representing effects of experimental parameters on the axial length of the magnetic nanorods. Statistically significant *p*-values are underlined.

Source	DF	Adjusted SS	Adjusted MS	F-value[a]	*p*-value
Model	6	83,496	13,916	3.22	0.022
Linear	3	34,058	11,353	2.62	0.079
A	1	5674	5674	1.31	0.266
B	1	3050	3050	0.71	0.411
C	1	24,535	24,535	5.67	0.027
Square	1	16,697	16,697	3.86	0.063
C^2	1	16,697	16,697	3.86	0.063
2-way interaction	2	33,434	16,717	3.87	0.038
AC	1	13,156	13,156	3.04	0.096
BC	1	20,278	20,278	4.69	0.043
Error	20	86,498	4325		
Lack-of-fit	18	84,260	4681	4.18	0.220
Pure error	2	2238	1119		
Total	26	169,994			

DF: Degree of freedom. SS: Sum of squares. MS: Mean of squares. A: Reaction mixture temperature (in °C). B: Essential oil volume added (in mL). C: Stirring speed of the reaction mixture (in rpm).
[a] The value of the F-test for comparison of variance of the model with variance of residuals.

Reliability of this model was tested by analysis of variance (ANOVA) and the lack-of-fit test. Results of this analysis at $\alpha = 0.10$ are given in Table 2. The established response surface regression model was statistically significant and included the following terms: A ($p = 0.266$), B ($p = 0.411$), C ($p = 0.027$), C^2 ($p = 0.063$), AC ($p = 0.096$), and BC ($p = 0.043$). Terms A and B were kept in the model due to hierarchy of terms. The experimental parameter D, *i.e.,* N_2 flow rate that passed through the reaction mixture, was found to be statistically insignificant for the system. The R^2 value of 49.1% was fair; its value measures how close the response surface model fits the data but not its adequacy. The *p*-value for the *lack-of-fit* test value was higher than $\alpha = 0.10$ ($p = 0.220$) and hence, statistically insignificant. Therefore, it was concluded that there was no reason to reject the model, and that it adequately fits the data.

To verify *the goodness-of-fit* of this response surface regression model, the residuals (differences between the measured values and the values predicted by the model) were examined. Distribution of residuals were equally distributed around zero (Fig. 2A). Residuals were not correlated with the run order, and no unusual structures or patterns were observed except for two outliers (nos. 1 and 9) (Fig. 2B). These results confirmed the *goodness-of-fit* of the model with the empirical data.

3.2. The effect of the experimental parameters and the selection of experimental parameters providing the synthesis of small-sized nanorods

Fig. 3 shows the effects of the experimental parameters included in the response surface regression model, *i.e.* reaction mixture temperature used for synthesis (A), *S. hispanica* essential oil volume (B), and stirring of speed of the reaction mixture (C). Increasing the temperature of the reaction mixture resulted in a linear reduction in the size of the magnetic nanorods. This was likely due to higher temperature resulting in faster and more effective reduction of the magnetic nanostructure precursors at the interface of two phases. Increasing the volume of essential oil added to the reaction mixture also resulted in a linear decrease in the size of the magnetic nanorods. Likely, this was due to an increase in the amount of crystallization seeds at the interfacial layer between the solution and essential oil. Finally, it was also observed that low stirring speed or no stirring of the reaction mixture contributed to the formation of smaller magnetic nanorods. Presumably, this was because capping and stabilizing properties of compounds included in *S.*

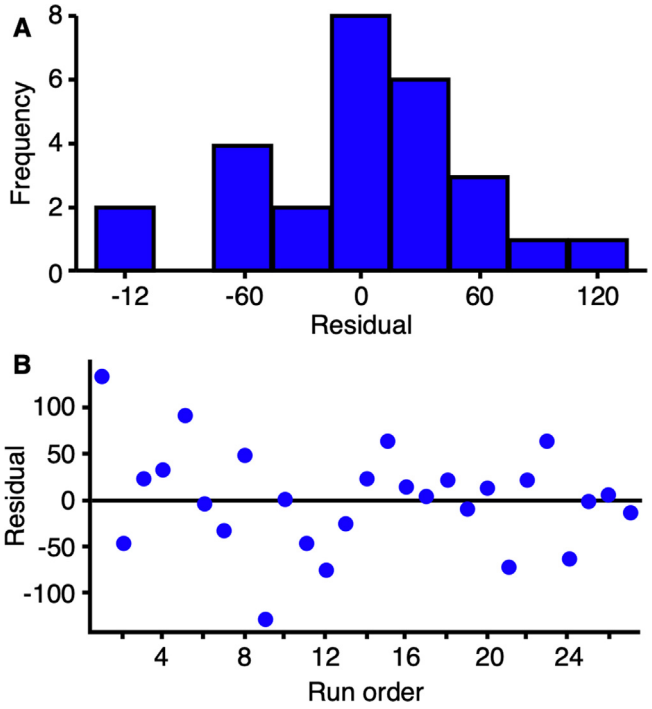

Fig. 2. (A) A frequency distribution graph of residuals, and (B) a scatter plot of residuals versus the run order.

hispanica essential oil were much better when it was not homogeneously dispersed in the solution.

Considering the developed model, it was established that magnetite nanorods with axial length of 3.0 nm, as measured by DLS, could be produced under the following conditions: A = 91 °C, B = 4.8 mL, and C = 0 rpm.

To validate this prediction, the synthesis of magnetic nanorods was independently carried out, maintaining optimal experimental conditions established on the basis of the developed response surface regression model, *i.e.,* using 4.8 mL of essential oil, keeping the reaction mixture temperature at 91 °C, and leaving the reaction mixture unstirred. Magnetite nanorods produced using the mentioned experimental conditions were collected by magnetic decantation, and then subjected to analysis by DLS to acquire the average size in reference to their axial length. A very good agreement between the mean value (n = 3) of the measured size of the magnetic nanorods synthesized in these conditions and the value obtained at optimal conditions predicted on the basis of the model was achieved. The relative error between both values was 15%.

3.3. Characterization of the granulometric properties of magnetic nanorods synthesized under optimal experimental conditions

TEM was used to assess the granulometric properties of the magnetic nanorods produced under the optimal experimental conditions. The resultant magnetic nanostructures were well dispersed with visible grain boundaries (Fig. 4A–C). As was expected, all nanostructures synthesised in these conditions were rod shaped (Fig. 4A–C). The average axial length and diameter were 43.4 ± 20.5 nm and 3.6 ± 0.9 nm, respectively. The aspect ratio (length to diameter) of the synthesized nanorods was 12.1 ± 5.2 nm. EDX analysis was conducted to reveal the elemental composition of the synthesized magnetite nanorods (Fig. 4D). Presence of Fe and O was confirmed. Furthermore, C (from the sample holder), Cu (from the Cu grid), and Cl (from magnetic nanorods precursors) were detected as well.

To confirm formation of crystalline magnetite nanostructures, SAED and XRD measurements were carried out. As shown in Fig. 5A, the ring SAED pattern was detected with *d*-spacing values of 2.797, 2.614, 2.053, and 1.724 Å. These *d*-spacing values corresponded to (2 2 0), (3 1 1), (4 0 0), and (4 2 2) Miller indices and were characteristics for Fe_3O_4 nanostructures [38,39]. A *d*-spacing value of 2.780 Å, which corresponds to the (3 2 1) plane of γ-Fe_2O_3 magnetic nanostructures, was not detected in the acquired SAED pattern. This pointed out that the fabricated magnetic nanostructures were Fe_3O_4 and not Fe_2O_3 [38]. Similar conclusions were drawn from the XRD pattern. As seen in Fig. 5B, reflection peaks at 2Θ values of 31.0, 35.3, 43.1, and 53.2°, corresponding to diffractions of (2 2 0), (3 1 1), (4 0 0), and (4 2 2), can be identified [20]. The measured XRD pattern of the resultant magnetic nanostructures additionally matched the pattern of the Fe_3O_4 standard (JCPDS, card no. 19-0629). Additional peaks that were identified, *i.e.,* at 20.8° of 2Θ, were likely associated with the presence of polyphenols from the *S. hispanica* essential oil. Additionally, the several peaks that occurred at 23-26° of 2Θ were possibly related to the presence of iron oxohydrooxide (FeOOH) formed by oxidation of Fe(II) ions during the synthesis of magnetite nanostructures [14]. Based on the SAED and XRD measurements, it was concluded that Fe_3O_4 nanorods (with a cubic inverse spinel structure) were produced by green synthesis with *S. hispanica* essential oil.

3.4. Characterization of magnetic properties of magnetic nanorods synthesized under optimal experimental conditions

To examine the magnetic properties of the nanostructures produced under the optimal experimental conditions, SQUID measurements were carried out. The temperature dependence of the inverse magnetic susceptibility (right-hand side axis) and magnetic susceptibility (left-hand side axis) of nanocrystalline Fe_3O_4 nanorods in a weak applied external magnetic field $\mu_0 H$ = 50 Oe are presented in Fig. 6A. Above ~25 K, the

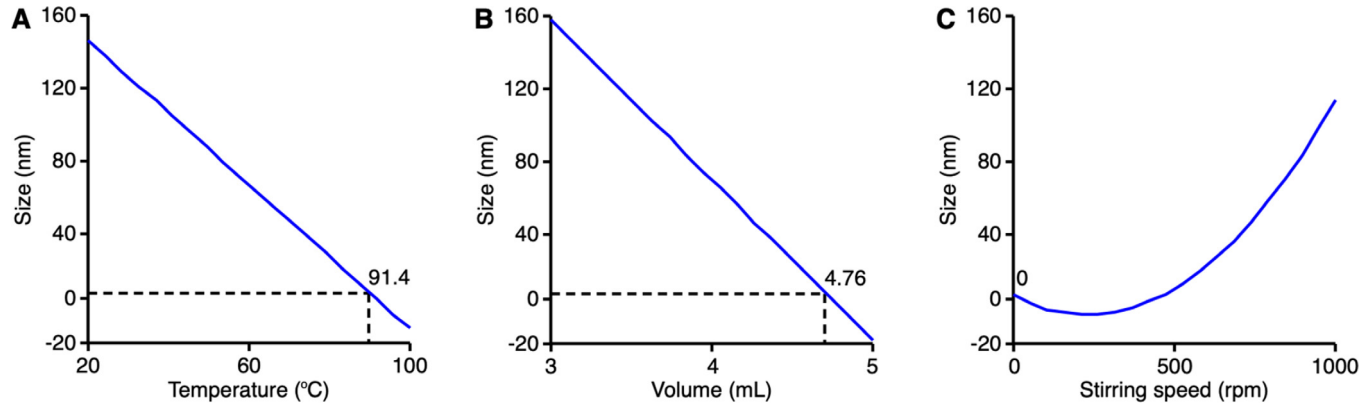

Fig. 3. The effect of the significant experimental parameters along with the optimal conditions for production of ~3 nm magnetic nanorods. (A) Reaction mixture temperature (in °C). (B) Essential oil volume (in mL). (C) Stirring speed of the reaction mixture (in rpm).

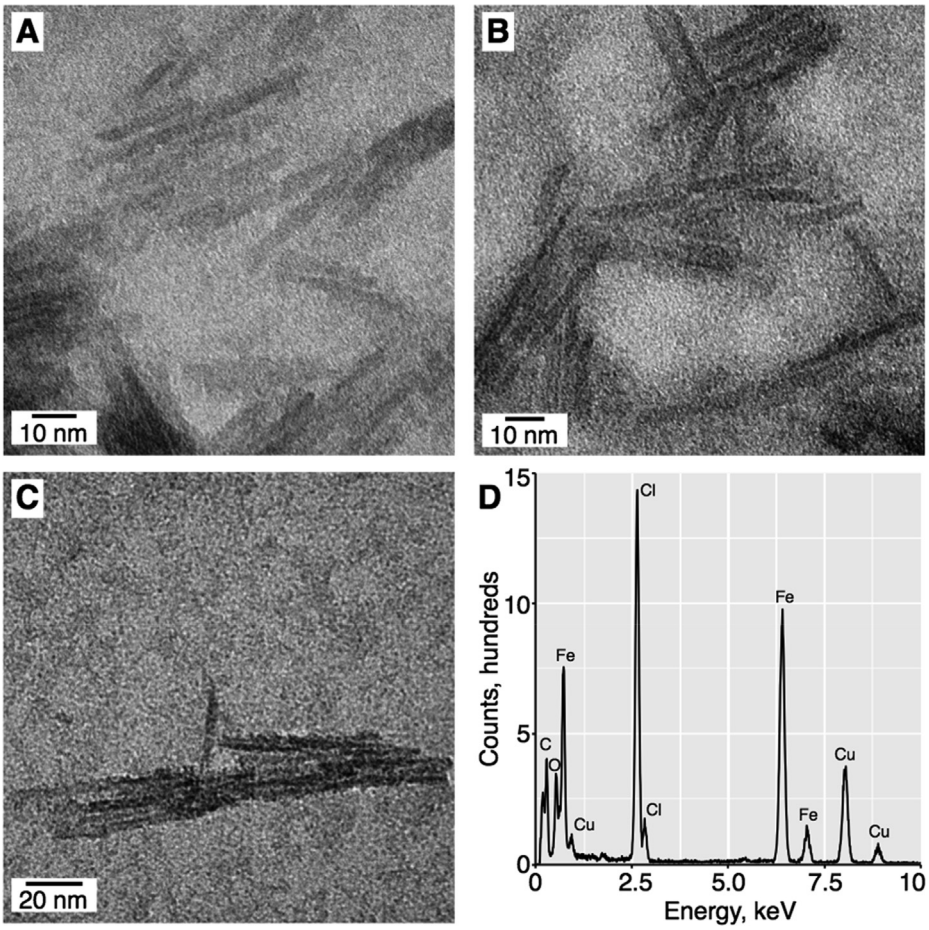

Fig. 4. Morphology of the magnetic nanostructures produced under the optimal synthesis conditions. (A–C) Representative TEM micrographs. (D) The EDX spectrum.

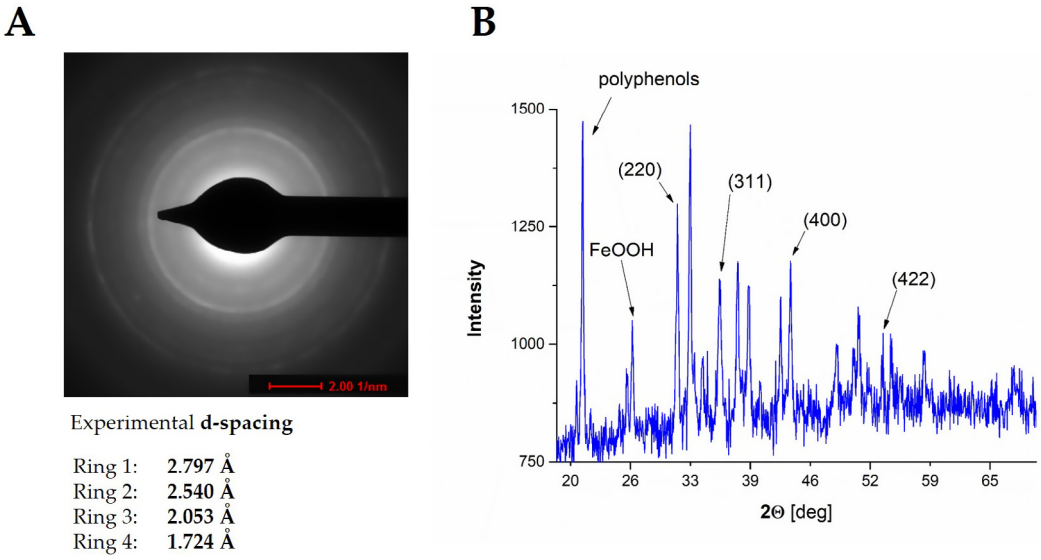

Fig. 5. Structural properties of the magnetic nanorods determined using (A) SAED and (B) XRD.

conventional Curie-Weiss law ($\chi(T) = C/(T - \Theta p)$) was obeyed with a Curie constant (C) of 25.57×10^{-3} emu K g^{-1} and paramagnetic Curie temperature (Θp) of 12.65 K.

Measured $\chi(T)$ variation did not show any clear anomaly or kink associated with Verwey transition for bulk magnetite expected at Verwey temperature (T_V) 120 K [39]. The observed behavior of $\chi(T)$ was in concert with that of the σ(H) isotherm taken at a temperature of 40 K (Fig. 6C). It implied that the nanorods displayed paramagnetic (or superparamagnetic) character when studied at high temperatures. The positive value of the Θp parameter points suggests predominantly ferromagnetic-like correlation between the magnetic moments in the material. This hypothesis was supported by the following two observations: i) distinct differences between curves collected in zero-field (ZF) and zero-field-cooling (FC) regimes (Fig. 6B) and ii) the narrow

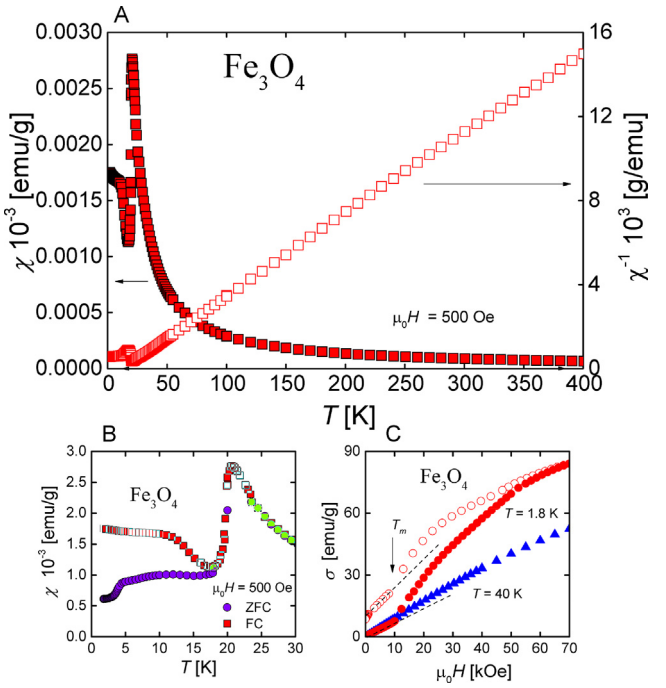

Fig. 6. (A) Temperature dependence of magnetic susceptibility (left-hand side axis) and inverse magnetic susceptibility (right-hand side axis) of the Fe_3O_4 nanorods measured in the field of $\mu_0H = 500$ Oe. The solid line is the Curie–Weiss fit described in the text. (B) Low-temperature magnetic susceptibility data taken upon cooling the material in zero (ZFC) and applied (FC) fields. (C) Magnetic field variation of magnetization measured at 1.8 K and 40 K with increasing (filled symbols) and decreasing (open symbols) magnetic field strength. The straight dashed lines emphasize linear behavior of $\sigma(\mu_0H)$ at 1.8 K.

and tall magnetic hysteresis, with small remanence of 0.013 emu g^{-1}, in field dependence of magnetization up to about 55 kOe at a temperature of 1.8 K (Fig. 6C). According to the literature [39], this type of magnetic interactions in magnetite arises from an imbalance of octahedral and tetrahedral sublattices of iron cations in their inverse spinel structure. The morphology of magnetic nanorods strongly affects the magnetic properties of the material, for which maximum nanoparticle sizes are about 38–54 nm [39,40]. For the magnetic nanorods characterized here, with average length of 43.4 ± 20.5 nm and diameter of 3.6 ± 0.9 nm, the axial length was at the border of the characteristic length for single domain particles. At this base, one could expect multiple domains separated by domain walls with magnetic moments aligned to one direction inside each domain. Indeed, at a low temperature regime, where deviation $\chi(T)^{-1}$ from the Curie-Weiss law is observed, one could find a couple of characteristic features of magnetic behavior (Fig. 6B). At temperatures higher than the bifurcation temperature (T_{bf}) of 18 K, no difference between ZFC and FC magnetic susceptibility curves was observed. Both curves were independent of magnetic history of the material; that is, both curves were identical on heating and cooling in the same applied field within experimental error. At T_m = 21 K, magnetic susceptibility $\chi(T)$ formed a sharp cup-like feature, which resembled what occurs, for example, in spin-glass, superparamagnetic, mictomagnetic, and simply AFM systems [41,42]. Previously, a similar in shape anomaly at higher temperatures of 28 K and 92 K was reported for 5–7 nm diameter magnetite nanostructures coated with oleic acid and a silica shell, respectively, and described as a fingerprint of superparamagnetic behavior [43,44]. However, this anomaly is sharp and quite asymmetric for the nanorods characterized here, unlike the typical broad anomaly owing to transition of isolated magnetic moments, for which clustering [45] or long-range correlation can be ignored [41,42]. Finally, below T_{max}, the FC curve did not saturate as could be expected for simple spin-glass systems, but instead it significantly dropped. This suggested strong collective antiferromagnetic correlation typical for short-range spin glass-like (mictomagnetic) states or simple AFM orderings [41,42]. Consistently, the magnetization curve $\sigma(\mu_0H)$, taken at a temperature of 1.8 K with increasing (full symbols) and decreasing (open symbols) magnetic field strength, exhibited nearly linear behavior up to 10 Oe (referred to as T_m in Fig. 6C), followed by metamagnetic-like features in stronger magnetic fields.

To support the presence of the antiferromagnetic correlation hypothesis, it is worthwhile recalling that all inter-atomic interactions in magnetite are antiferromagnetic and that the value of the exchange constant J predominantly depends on the bond angle Fe–O–Fe, which can be strongly affected by finite-size and surface effects [39]. Furthermore, strong dependence of the antiferromagnetic sticking force due to coating of a surfactant on particles having a large surface area to volume ratio have recently been demonstrated for Na-oleate coated Fe_3O_4 nanoparticles by means of electron paramagnetic resonance (EPR) [46].

Signatures of nonergodicity were clearly observed below the bifurcation temperature $T_{bf} = 18$ K, where both ZFC and FC curves were split from each other and behaved in dissimilar manners upon further cooling (Fig. 6B). With decreasing temperature, the ZFC curve firstly became nearly featureless with a value of 1×10^{-3} emu g^{-1}, then it rapidly dropped off at temperature ~4.8 K to a value of 0.6×10^{-3} emu g^{-1}. On the contrary, FC data started to gently increase with decreasing temperature, then finally at 10 K it showed some tendency to saturate at an enhanced value of about 1.7×10^{-3} emu g^{-1}. This feature clearly indicated a magnetic origin of the observed anomaly at 4.8 K, pointing to some rearrangement or freezing of the magnetic moments [47]. On the other hand, considering the extensive homogeneity range for nanorods, an extrinsic nature of the anomaly at 4.8 K could not be completely excluded. Neutron-diffraction or Mossbauer experiments would be necessary to clarify the origin of the observed feature.

Finally, as can be inferred from Fig. 6C, at low temperatures, magnetization $\sigma(\mu_0H)$ curves did not fully saturate even in the strongest magnetic field applied. It might be thus concluded that the magnetic moments of the magnetic nanostructures were not perfectly parallel to the applied magnetic field. At 1.8 K and μ_0H = 70 kOe, magnetization reached a value of ~83 emu g^{-1} that was much larger than, for example, magnetization of previously reported magnetite nanostructures (66.2 emu g^{-1}) [48], one-dimensional Ag-Fe_3O_4 core-shell heteronanowires (5.7–26.4 emu g^{-1}) [49], or single-crystalline nanowires of Fe_3O_4 with a diameter of 35 nm and a length of about 0.48 nm (about 47 emu g^{-1}) [50]. On the other hand, the established value of magnetization was comparable to other Fe_3O_4 nanorods (82.6 emu g^{-1}) [50] and only slightly smaller than this obtained for bulk magnetite (92–100 emu g^{-1}) [39]. In particular, comparable values of magnetic saturation of Fe_3O_4 nanorods described here and elsewhere [50] indicated negligible mass of the reducing and capping agents originated from *S. hispanica* essential oil used here. In turn, the open hysteresis loop up to 50 KOe suggested a large spin disorder (spin canting) at the surface with multiple stable configurations, as was previously observed for nanoparticles such as $NiFe_2O_4$ and $(Fe_{0.26}Ni_{0.74})_{50}B_{50}$ [51,52].

3.5. The role of chemical compounds in the synthesis of magnetic nanorods

ATR FT-IR spectroscopy was used to identify chemical compounds in *S. hispanica* essential oil that might contribute to the formation and stabilization of magnetic nanorods, as well as to evaluate interactions between functional groups of these components and the surface of produced magnetite nanostructures. ATR FT-IR spectra for pure *S. hispanica* essential oil (Fig. 7A) and for magnetic nanorods synthesized under optimal synthesis conditions (Fig. 7B) were compared.

In the ATR FT-IR spectrum of *S. hispanica* essential oil, stretching

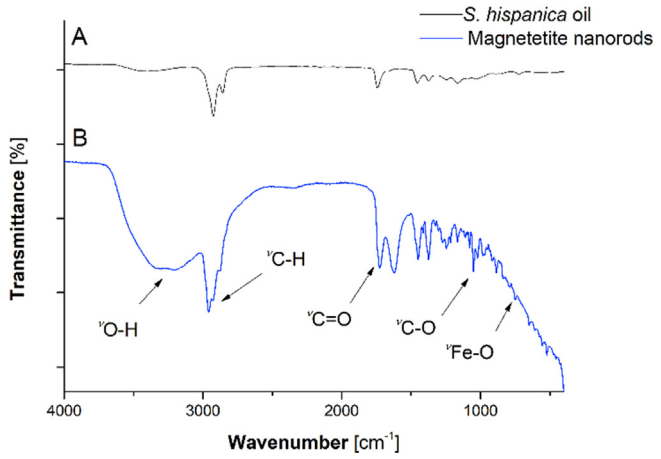

Fig. 7. (A) The ATR FT-IR spectrum of pure *S. hispanica* essential oil. (B) The ATR FT-IR spectrum of the solution of magnetite nanorods synthesized under optimal experimental conditions.

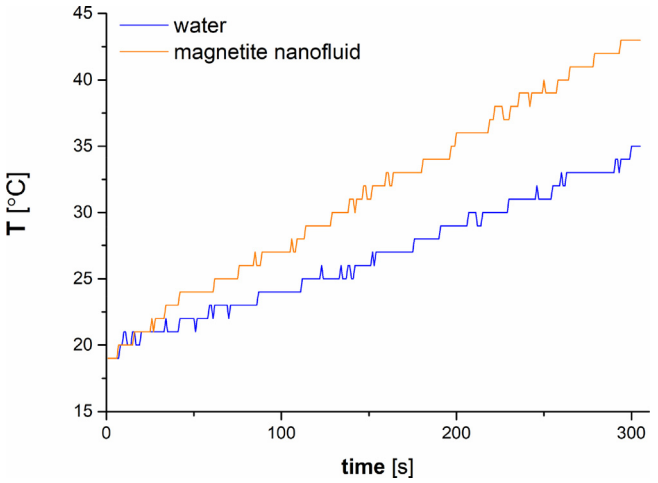

Fig. 8. Microwave-induced changes in the temperature of water and the synthesized magnetic nanofluid.

and deformation vibrations of the main functional groups were identified and assigned to the presence of typical terpenoid derivatives (Fig. 7A, Table 3). The intense absorption band at 3396 cm^{-1} was associated with the symmetric stretching vibrations ν of the –OH group of water molecules [53]. Intense absorption bands at 2926 cm^{-1} and 2856 cm^{-1} were associated with symmetric and asymmetric stretching vibrations ν of the aliphatic methylene group of terpenes such as β-pinene and β-caryophyllene [54–56]. The intense absorption band at 1454 cm^{-1} was assigned to C–H stretching vibration ν of terpenes such as β-pinene and camphor [54,55]. The absorption band at 1373 cm^{-1} was associated with deforming vibrations δ of methyl and methylene groups of β-pinene [57]. Twisting and wagging out-of-plane bending vibrations γ of the methylene group of β-caryophyllene were identified on the basic of the absorption band at 887 cm^{-1} [55,58]. The absorption band at 1741 cm^{-1} was associated with C=O stretching vibration ν of the ester functional group, and might be associated with the presence of monoterpenes like β-thujone [54,57]. All together, these bands might suggest the occurrence of terpenes such as β-pinene, β-caryophyllene, camphor, and β-thujone in the *S. hispanica* essential oil and its solutions [54]. In the solution of magnetic nanorods, a band at 555 cm^{-1} was identified and likely corresponded to the metal–oxygen Fe-O bond [59] (Fig. 7B, Table 3). This bond is characteristic for synthesis of magnetite nanostructures [8,59,60], and confirms the production of magnetic nanorods. Furthermore, in this case, symmetric stretching vibrations (ν) of the OH group at 3203 cm^{-1} were detected in addition to the bending vibrations of the –OH group corresponding to the one excessive peak at 1621 cm^{-1}. The latter is related to the bending vibration of the adsorbed water molecule in the amorphous portion of the magnetite surface [53].

Overall, the ATR FT-IR spectra suggested that terpenes such as β-pinene, camphor, β-thujone, and β-caryophyllene present in the *S. hispanica* essential oil were responsible for the synthesis and surface functionalization of magnetic nanorods.

3.6. Thermal behavior of magnetite nanorods in dielectric heat

Magnetic nanostructures respond to an electromagnetic field by aligning along field lines, which leads to enhancing heat transfer [61]. For this reason, it was expected that the synthesized nanorods could reveal an improved magnetic response when exposed to concentrated microwaves that would be quite a valuable feature, for example, in breast cancer imaging. Because magnetic excitation strongly influences the temperature of magnetite nanofluids, the thermal behavior of the magnetite nanofluid synthesized under the optimal experimental conditions was determined and compared to this assessed for water. Fig. 8 displays the recorded temperature changes observed for water and the magnetic nanofluid resulting from irradiation with an electromagnetic field of microwave radiation.

Water, due to its dipole momentum, is considered a very good absorber of microwaves. Despite that, as can be seen in the Fig. 8, the solution containing magnetic nanorods displayed a larger temperature increase in response to microwave radiation as compared to water. Accordingly, the magnetic nanofluid reached a temperature of 43 °C, whereas water reached a temperature of just 35 °C. Importantly, microwave heating of the nanostructures resulted in a faster rate of heating, referred to as k(h) (see Section 2.6.). Values of k(h) of the

Table 3
Absorption bands identified in the ATR FT-IR spectra.

Band assignments	*S. hispanica* essential oil [cm^{-1}]	*S. hispanica* essential oil with Fe_3O_4 nanorods [cm^{-1}]
Symmetric stretching (ν) vibration of O–H	3396	3203
Asymmetric and symmetric stretching vibration (ν) of C–H	2926	2960
	2859	2929
Stretching vibration (ν) of C=O	1741	1727
Bending vibration of O–H		1621
In-plane bending vibrations (δ) of CH_2 and CH_3	1454	1450
In-plane bending vibration (δ) of CH_2	1373	1374
Stretching vibration (ν) of the C–O or C–C	1244	1246
	1166	
Bending vibration (δ) of C–O–H	1094	1051
Wagging (ω) vibration of the CH_2	887	886
Stretching vibration (ν) of Fe–O		555
		521

magnetic nanofluid and water were $12.2 \times 10^{-3}\,s^{-1}$ and $8.4 \times 10^{-3}\,s^{-1}$, respectively. These observations indicated that the synthesized magnetic nanofluid was indeed electromagnetically excited. Moreover, it was consistent with literature reports [10,25], where magnetite nanoparticles were indicated as very convenient contrasting agents for breast cancer microwave imaging due to ease of electromagnetic excitation. Based on these data, it was presumed that the magnetite nanorods synthesized here might also be useful for this medical purpose.

4. Conclusions

DOE along with RSM were applied to evaluate the contribution of selected experimental parameters on the granulometric properties of magnetic nanorods produced with the aid of *S. hispanica* essential oil. It was found that the reaction mixture temperature, the volume of essential oil, and the stirring speed had significant impacts on the size of the produced magnetic nanorods. Under optimal experimental conditions (reaction mixture temperature of 91 °C, essential oil volume of 4.8 mL, and a speed of stirring of 0 rpm) that provided production of ~3 nm nanostructures, the nanostructures exhibited an average axial length of 43.4 ± 20.5 nm, diameter of 3.6 ± 0.9 nm, and an aspect ratio of 12.1 ± 5.2 nm. The elemental composition of the resulting magnetic nanorods was estimated by EDX, while their crystalline structure was determined by SAED and XRD, respectively. It was confirmed that magnetite nanostructures were formed with a crystalline cubic inverse spinel structure. These nanorods exhibited complex magnetic behavior with coexistence of ferr- and antiferromagnetic and spin-glass-like behavior, typical for mictomagnets. Based on ATR FT-TR, it was established that terpenes-like compounds were likely involved in the green synthesis and surface functionalization of the abovementioned magnetite nanorods. It was also shown that the synthesized nanostructures were susceptible to microwave-excitation. After appropriate adjustments, they might be useful as a contrast agent for microwave-imaging of tissues.

We believe that this procedure allows for the production of defined materials not only for the bioengineering applications described within the manuscript, but also for biotechnology applications including, for example, magnetic drug targeting. In this case, the magnetic nanomaterials should be as small as possible to improve tissular diffusion, and should be stabilized by biocompatible capping agents [62]. The magnetic nanorods produced within this work have these properties, *i.e.* there are small in size (an average axial length of 43.4 ± 20.5 nm, diameter of 3.6 ± 0.9 nm, and aspect ratio of 12.1 ± 5.2 nm), their surface is functionalized by several terpenes such as β-pinene, β-caryophyllene, camphor, and β-thujone origining from *S. hispanica* essential oil, and they exhibit glass-like (mictomagnetic) behavior with both ferro- and antiferromagnetic interactions. In future work, it would be interesting to examine whether the use of essential oils isolated from *S. hispanica* grown to different maturity stages influences the properties of the produced nanorods.

Acknowledgements

We would like to thank Dr. Anna Lesniewicz for kindly performing the XRD measurements. This work was funded by a statutory activity subsidy from the Polish Ministry of Science and Higher Education for the Faculty of Chemistry of Wroclaw University of Science and Technology (Poland). Anna Dzimitrowicz is supported by the Foundation for Polish Science (FNP), program START 022.2018. George diCenzo is supported by a Natural Sciences and Engineering Research Council of Canada Post-Doctoral Fellowship.

Conflicts of interest

The authors declare no conflict of interest.

References

[1] R.W. Kelsall, I.W. Hamley, M. Geoghegan, Nanoscale Science and Technology, John Wiley and Sons Ltd, West Sussex, England, 2008.
[2] C. Prasad, S. Karlapudi, P. Venkateswarlu, I. Bahadur, S. Kumar, Green arbitrated synthesis of Fe_3O_4 magnetic nanoparticles with nanorod structure from pomegranate leaves and Congo red dye degradation studies for water treatment, J. Mol. Liq. 240 (2017) 322–328.
[3] X. Mou, Z. Ali, S. Li, N. He, Applications of magnetic nanoparticles in targeted drug delivery system, J. Nanosci. Nanotechnol. 15 (2015) 54–62.
[4] I. Koh, L. Josephson, Magnetic nanoparticle sensors, Sensors 9 (2009) 8130–8145.
[5] M. Neamtu, C. Nadejde, V.D. Hodoroaba, R. Schneider, L. Verestiuc, U. Panne, Functionalized magnetic nanoparticles: synthesis, characterization, catalytic application and assessment of toxicity, Sci. Rep. 8 (2018) 6278.
[6] B.D. Terris, T. Thomson, Nanofabricated and self-assembled magnetic structures as data storage media, J. Phys. D Appl. Phys. 38 (2005) R199.
[7] M. Latorre, C. Rinaldi, Applications of magnetic nanoparticles in medicine: magnetic fluid hyperthermia, P. R. Health Sci. J. 28 (2009) 227–238.
[8] M. Mahdavi, F. Namvar, M.B. Ahmad, R. Mohamad, Green biosynthesis and characterization of magnetic iron oxide (Fe_3O_4) nanoparticles using seaweed (*Sargassum muticum*) aqueous extract, Molecules 18 (2013) 5954–5964.
[9] L. Fass, Imaging and cancer: a review, Mol. Oncol. 2 (2008) 115–152.
[10] P.M. Meaney, M.W. Fanning, T. Raynolds, C.J. Fox, Q. Fang, C.A. Kogel, S.P. Poplack, K.D. Paulsen, Initial clinical experience with microwave breast imaging in women with normal mammography, Acad. Radiol. 14 (2007) 207–218.
[11] K.R. Foster, H.P. Schwan, Dielectric properties of tissues and biological materials: a critical review, Crit. Rev. Biomed. Eng. 17 (1989) 25–104.
[12] A. Demir, R. Topkaya, A. Baykal, Green synthesis of superparamagnetic Fe_3O_4 nanoparticles with maltose: its magnetic investigation, Polyhedron 65 (2013) 282–287.
[13] H.Y. El-Kassas, M.A. Aly-Eldeen, S.M. Gharib, Green synthesis of iron oxide (Fe_3O_4) nanoparticles using two selected brown seaweeds: characterization and application for lead bioremediation, Acta Oceanol. Sin. 35 (2016) 89–98.
[14] S. Groiss, R. Selvaraj, T. Varadavenkatesan, R. Vinayagam, Structural characterization, antibacterial and catalytic effect of iron oxide nanoparticles synthesized using the leaf extract of *Cynometra ramiflora*, J. Mol. Struct. 1128 (2017) 572–578.
[15] S. Hsieh, B.H. Huang, S.L. Hsieh, C.C. Wu, C.H. Wu, P.Y. Lin, Y.S. Huang, C.W. Chang, Green fabrication of agar-conjugated Fe_3O_4 magnetic nanoparticles, Nanotechnology 21 (2010) 445601.
[16] V.C. Karade, P.P. Waifalkar, T.D. Dongle, S.C. Sahoo, P. Kollu, P.S. Patil, P.B. Patil, Greener synthesis of magnetite nanoparticles using green tea extract and their magnetic properties, Mater. Res. Express 4 (2017) 096102.
[17] K. Manquian-Cerda, E. Cruces, M.A. Rubio, C. Reyes, N. Arancibia-Miranda, Preparation of nanoscale iron (oxide, oxyhydroxides and zero-valent) particles derived from blueberries: reactivity, characterization and removal mechanism of arsenate, Ecotoxicol. Environ. Saf. 145 (2017) 69–77.
[18] F. Namvar, S.H. Rahman, R. Mohamad, J. Bahavara, M. Mahdavi, E. Amini, M.S. Chartrand, S.K. Yeap, Cytotoxic effect of magnetic iron oxide nanoparticles synthesized via seaweed aqueous extract, Int. J. Nanomed. 9 (2014) 2479–2488.
[19] C. Prasad, K. Sreenivasulu, S. Gangadhara, P. Venkateswarlu, A facile green synthesis of spherical Fe_3O_4 magnetic nanoparticles and their effect on degradation of methylene blue in aqueous solution, J. Mol. Liq. 221 (2016) 993–998.
[20] C. Prasad, S. Gangadhara, P. Venkateswarlu, Bio-inspired green synthesis of Fe_3O_4 magnetic nanoparticles using watermelon rinds and their catalytic activity, Appl. Nanosci. 6 (2016) 797–802.
[21] N. Sangeetha, A.K. Kumaraguru, Antitumor effects and characterization of biosynthesized iron oxide nanoparticles using seaweeds of gulf of mannar, Int. J. Pharm. Pharm. Sci. 7 (2014) 469–476.
[22] S. Venkateswarlu, B.N. Kumar, B. Prathima, Y. SubbaRao, N.V.V. Jyothi, A novel green synthesis of Fe_3O_4 magnetic nanorods using *Punica granatum* rind extract and its application for removal of Pb (II) from aqueous environment, Arab. J. Chem. (2014), https://doi.org/10.1016/j.arabjc.2014.09.006.
[23] Z. Wang, C. Fang, M. Mallavarapu, Characterization of iron–polyphenol complex nanoparticles synthesized by Sage (*Salvia officinalis*) leaves, Environ. Technol. Innovat. 4 (2015) 92–97.
[24] S. Geng, H. Yang, X. Ren, Y. Liu, S. He, J. Zhou, Na. Su, Y. Li, Ch. Xu, X. Zhang, Z. Cheng, Anisotropic magnetite nanorods for enhanced magnetic hyperthermia, Chem. Asian J. 11 (2016) 2996–3000.
[25] B. Bellizzi, O.M. Bucci, I. Catapano, Microwave cancer imaging exploiting magnetic nanoparticles as contrast agent, IEEE Trans. BioMed. Eng. 58 (2011) 2528–2536.
[26] N. Mohd Ali, S.K. Yeap, W.Y. Ho, B.K. Beh, S.W. Tan, S.G. Tan, The promising future of chia, *Salvia hispanica* L, J. Biomed. Biotechnol. (2018), https://doi.org/10.1155/2012/171956.
[27] M. Ahmed, I.P. Ting, R.W. Scora, Leaf oil composition of *Salvia hispanica* L. from three geographical areas, J. Essent. Oil Res. 6 (1994) 223–228.
[28] B. Thomas, B. Vithiya, T. Prasad, S.B. Mohamed, C.M. Magdalane, K. Kaviyarasu, M. Maaza, Antioxidant and photocatalytic activity of aqueous leaf extract mediated green synthesis of silver nanoparticles using *Passiflora edulis* f. flavicarpa, J. Nanosci. Nanotechnol. 19 (2009) 2640–2648.
[29] A.A. Ezhilarasi, J.J. Vijaya, K. Kaviyarasu, M. Maaza, A. Ayeshamariam, L.J. Kennedy, Green synthesis of NiO nanoparticles using *Moringa oleifera* extract and their biomedical applications: Cytotoxicity effect of nanoparticles against HT-29 cancer cells, J. Photochem. Photobiol. B 164 (2016) 352–360.
[30] C.M. Magdalane, K. Kaviyarasu, J.J. Vijaya, B. Siddhardha, B. Jeyaraj, Photocatalytic activity of binary metal oxide nanocomposites of CeO_2/CdO

nanospheres: investigation of optical and antimicrobial activity, J. Photochem. Photobiol. B 163 (2016) 77–86.
[31] K. Kaviyarasu, C.M. Magdalane, K. Kanimozhi, J. Kennedy, B. Siddhardha, E.S. Reddy, N.K. Rotte, C.S. Sharma, F.T. Therma, D. Letsholathebe, G.T. Mola, M. Maaza, Elucidation of photocatalysis, photoluminescence and antibacterial studies of ZnO thin films by spin coating method, J. Photochem. Photobiol. B 173 (2017) 466–475.
[32] S.K. Jesudoss, J.J. Vijaya, L.J. Kennedy, P.I. Rajan, H.A. Al-Lohedan, R.J. Ramalingam, K. Kaviyarasu, M. Bououdina, Studies on the efficient dual performance of $Mn_{1-x}Ni_xFe_2O_4$ spinel nanoparticles in photodegradation and antibacterial activity, J. Photochem. Photobiol. B 165 (2016) 121–132.
[33] J.J. Vijaya, N. Jayaprakash, K. Kombaiah, K. Kaviyarasu, L.J. Kennedy, R.J. Ramalingam, K.A. Al-Lohedan, V.M. ManSoor-Ali, M. Maaza, Bioreduction potentials of dried root of *Zingiber officinale* for a simple green synthesis of silver nanoparticles: antibacterial studies, J. Photochem. Photobiol. B 177 (2017) 62–68.
[34] W. Cai, J. Wan, Facile synthesis of superparamagnetic magnetite nanoparticles in liquid polyols, J. Colloid Interface Sci. 305 (2007) 366–370.
[35] M. Bonini, A. Wiedenmann, P. Baglioni, Synthesis and characterization of surfactant and silica-coated cobalt ferrite nanoparticles, Physica A Stat. Mech. Appl. 339 (2004) 86–91.
[36] S.W. Provencher, CONTIN: a general purpose constrained regularization program for inverting noisy linear algebraic and integral equations, Comput. Phys. Commun. 27 (1982) 229–324.
[37] L.C. Burmeister, Convective Heat Transfer: Solutions Manual, John Wiley and Sons Ltd, West Sussex, England, 1993.
[38] I.M. Obaidat, C. Nayek, K. Manna, G. Bhattacharjee, I.A. Al-Omari, A. Gismelseed, Investigating exchange bias and coercivity in Fe_3O_4–γ-Fe_2O_3 core–shell nanoparticles of fixed core diameter and variable shell thicknesses, Nanomaterials 7 (2017) 415.
[39] J.M.D. Coey, Magnetic Properties of Iron in Soil Iron Oxides and Clay Mineral, Springer, Dordrecht, Neatherlands, 1988.
[40] J. Wang, Q. Chen, C. Zeng, B. Hou, Magnetic field induced growth of single crystalline Fe_3O_4 nanowires, Adv. Mater. 16 (2004) 137–140.
[41] S. Majetich, Processing, Properties, and Applications, North Carolina, USA, 2007.
[42] M.J. Benitez, O. Petracic, E.L. Salabas, F. Radu, H. Tuysuz, F. Schuth, H. Zabel, Evidence for core-shell magnetic behavior in antiferromagnetic Co_3O_4 nanowires, Phys. Rev. Lett. 101 (2008) 097206.
[43] K. Chesnel, M. Trevino, Y. Cai, J.M. Hancock, S.J. Smith, R.G. Harrison, Particle size effects on the magnetic behaviour of 5 to 11 nm Fe_3O_4 nanoparticles coated with oleic acid, J. Phys. Conf. Ser. 521 (2014) 012004.
[44] Y.P. He, S.Q. Wang, C.R. Li, Y.M. Miao, Z.Y. Wu, B.S. Zou, Synthesis and characterization of functionalized silica-coated Fe_3O_4 superparamagnetic nanocrystals for biological applications, J. Phys. D Appl. Phys. 38 (2005) 1342–1350.
[45] C. Djurberg, P. Svedlindh, P. Nordblad, M.F. Hansen, F. Bodker, S. Morup, Dynamics of an interacting particle system: evidence of critical slowing down, Phys. Rev. Lett. 79 (1997) 5154–5157.
[46] Y. Koseoglu, F. Yildiz, D.K. Kim, M. Muhammed, B. Aktaş, EPR studies on Na-oleate coated Fe_3O_4 nanoparticles, Phys. Stat. Sol. 12 (2004) 3511–3515.
[47] C. Echevarria-Bonet, D.P. Rojas, J.I. Espeso, J. Rodriguez Fernandez, L. Rodriguez Fernandez, P. Gorria, J.A. Blanco, M.L. Fdez-Gubieda, E. Bauer, G. Andr'e, L. Fernandez Barquin, Size-induced superantiferromagnetism with reentrant spin-glass behavior in metallic nanoparticles of $TbCu_2$, Phys. Rev. B 87 (2013) 180407(R).
[48] W. Wu, X. Xiao, S. Zhang, J. Zhou, L. Fan, F. Ren, C. Jiang, Large-scale and controlled synthesis of iron oxide magnetic short nanotubes: shape evolution, growth mechanism, and magnetic properties, J. Phys. Chem. C 114 (2010) 16092–16103.
[49] J. Ma, K. Wang, M. Zhan, Growth mechanism and electrical and magnetic properties of Ag–Fe_3O_4 core–shell nanowires, ACS Appl. Mater. Interfaces 7 (2015) 16027–16039.
[50] J. Wang, Y. Wu, Y. Zhu, Fabrication of complex of Fe_3O_4 nanorods by magnetic-field-assisted solvothermal process, Mater. Chem. Phys. 106 (2007) 1–4.
[51] R. Kodama, A.E. Berkowitz, Surface spin disorder in $NiFe_2O_4$ nanoparticles, Phys. Rev. Lett. 77 (1996) 394–397.
[52] E. de Biasi, C.A. Ramos, R.D. Zysler, H. Romero, Large surface magnetic contribution in amorphous ferromagnetic nanoparticles, Phys. Rev. B 65 (2002) 144416.
[53] G. Socrates, Infrared and Raman Characteristic Group Frequencies: Tables and Charts, John Wiley & Sons, 2004.
[54] G. Gudi, A. Kraahmer, H. Kruuger, H. Schulz, Attenuated total reflectance–Fourier transform infrared spectroscopy on intact dried leaves of sage (*Salvia officinalis* L.): accelerated chemotaxonomic discrimination and analysis of essential oil composition, J. Agric. Food Chem. 63 (2015) 8743–8750.
[55] H. Schulz, M. Baranska, Identification and quantification of valuable plant substances by IR and Raman spectroscopy, Vib. Spectrosc. 43 (2007) 13–25.
[56] T. Sato, Y. Ozaki, K. Iriyama, Molecular aggregation and photoisomerization of Langmuir-Blodgett films of azobenzene-containing long-chain fatty acids and their salts studied by ultraviolet-visible and infrared spectroscopies, Langmuir 10 (1994) 2363–2369.
[57] M.E. Rosas-Mendoza, J. Coria-Hernandez, R. Melendez-Perez, J.L. Arjona-Roman, Characteristics of chia (*Salvia hispanica* L.) seed oil extracted by ultrasound assistance, J. Mex. Chem. Soc. 61 (2017) 326–335.
[58] V. Arjunan, S. Subramanian, S. Mohan, Vibrational spectroscopic studies on trans-1, 4-polychloroprene, Turk. J. Chem. 27 (2003) 423–432.
[59] J.A. Lopez, F. Gonzalez, F.A. Bonilla, G. Zambrano, M.E. Gomez, Synthesis and characterization of Fe_3O_4 magnetic nanofluid, Rev. Latinoam. Metal. Mater. 30 (2010) 60–66.
[60] M. Klokkenburg, J. Hilhorst, B.H. Erne, Surface analysis of magnetite nanoparticles in cyclohexane solutions of oleic acid and oleylamine, Vib. Spectrosc. 43 (2007) 243–248.
[61] I. Nkurikiyimfura, Y. Wang, Z. Pan, Effect of chain-like magnetite nanoparticle aggregates on thermal conductivity of magnetic nanofluid in magnetic field, Exp. Therm. Fluid Sci. 44 (2013) 608–612.
[62] P. Tartaj, M.P. Morales, T. Gonzalez-Carreno, S. Veintemillas-Verdaguer, C.J. Serna, Advances in magnetic nanoparticles for biotechnology applications, J. Magn. Magn. Mater. 290 (2005) 28–34.